Increased reluctant vesicles underlie synaptic depression by GPR55 in axon terminals of cerebellar Purkinje cells

Takuma Inoshita[1] and Shin-ya Kawaguchi[1,*]

[1] Department of Biophysics, Graduate School of Science, Kyoto University
Oiwake-cho, Kitashirakawa, Sakyo-ku, Kyoto, 606-8502, Japan

*: Correspondence should be addressed to S. K.
e-mail: kawaguchi@nb.biophys.kyoto-u.ac.jp
Tel: 81-75-753-4200

Running Title
Synaptic suppression by GPR55 distinct from conventional CBRs

Keywords
cannabinoid, synaptic suppression, GPR55, synapse, Purkinje cell

Abstract

Control of synaptic transmission efficacy by neuronal activity and neuromodulators is pivotal for brain function. Synaptic suppression by cannabinoids activating CB1 receptors has been extensively studied at the molecular and cellular levels to understand the neuronal basis for symptoms of cannabis intake. Here, we focused on another type of cannabinoid receptor GPR55, which shows sensitivity to cannabidiol, a chemical included in cannabis, aiming to highlight its actions on presynaptic function. Taking advantage of direct patch-clamp recordings from axon terminals of cerebellar Purkinje cells together with fluorescent imaging of vesicular exocytosis using synapto-pHluorin, we show that GPR55 suppresses synaptic transmission as CB1 receptor does, but through a distinct presynaptic modulation of release machinery. Activation of GPR55 reduced transmitter release by changing neither presynaptic action potential waveform nor Ca^{2+} influx, but by making a large population of Ca^{2+}-responsive synaptic vesicles insensitive to Ca^{2+} influx through voltage-gated Ca^{2+} channels, leading to substantial reduction of the readily releasable pool of vesicles. Thus, the present study identifies a unique mechanism to suppress presynaptic transmitter release by atypical receptor for cannabinoid, which would enable subtype-specific modulation of neuronal computation by cannabinoid receptors.

Introduction

Neuronal communication at chemical synapses is central to information processing in the circuit, and its activity-dependent modulation provides adaptive change of the brain computation (Kandel, 2001). Short- and long-term changes of transmission efficacy at central synapses have been extensively studied in terms of molecular/cellular mechanisms and physiological significance, which have demonstrated their critical roles in learning and memory in animals (Abbott and Regehr, 2004). One of such modulations of synaptic strength is that by endocannabinoids (Kreitzer and Regehr, 2001; Ohno-Shosaku et al., 2001; Wilson and Nicoll, 2001; Diana et al., 2002), which is also related to the cellular and neuronal basis for actions of cannabis (Kano et al., 2009). One well-known synaptic modulation by cannabinoids is the activity-dependent short-term suppression of synaptic transmission, such as depolarization-induced suppression of excitation (DSE) and inhibition (DSI), caused by reduced transmitter release from presynaptic terminals as a result of activation of cannabinoid receptor type 1 (CB1). The CB1 activation is thought to decrease presynaptic Ca^{2+} influx upon an action potential (AP) arrival (Kreitzer and Regehr, 2001; Kushmerick et al., 2004; Wu et al., 2020).

In spite of the substantial efforts that have been made for unraveling cannabinoids' action on the nervous system, it still remains elusive whether the reduction of Ca^{2+} influx fully explains the suppression of transmission by cannabinoids or if other mechanisms, such as an altered release machinery, may also be involved generally at central synapses, as already suggested for CB1-mediated change of presynaptic vesicular docking (Ramirez-Franco et al., 2014). In addition, multiple types of molecules contained in cannabis are now known to act on the nervous system, and particularly one of them, cannabidiol, is attracting attention because of its potential preferred therapeutic actions on various neurological dysfunctions such as epilepsy and anxiety symptoms (Shallcross, et al., 2019; Devinsky, et al., 2024). GPR55, a cannabinoid receptor that has been identified as a potential target of cannabidiol (Baker et al., 2006; Oka et al., 2007), was recently reported to modulate synaptic transmission at glutamatergic and GABAergic synapses in the hippocampus (Rosenberg et al., 2023), although the detailed mechanism of action remains unclear. Thus, in spite of the large impact of synaptic modulation exerted by cannabinoids, the present knowledge about the mechanisms of their actions is quite limited.

To study in detail how cannabinoids modulate synaptic physiology, direct *tour-de-force* patch-clamp recordings of transmitter release at axon terminals, in combination with molecular biological methods and fluorescent imaging, would be a powerful technique. One preparation that is amenable to detailed biophysical analysis of transmitter release is the axon terminals of cerebellar Purkinje cells (PCs) (Kawaguchi & Sakaba, 2015). Taking advantage of the feasibility to perform direct PC axonal patch-clamp recordings in combination with fluorescent imaging of vesicular fusion in dissociated cultures and postsynaptic recordings from neurons in deep cerebellar nuclei (DCN) of slices, here we studied how the presynaptic release machinery is modulated by another type of cannabinoid receptor, GPR55, that is potentially expressed in PCs (Ryberg et al., 2007; Wu et al., 2013). We demonstrate

that GPR55 suppresses synaptic transmission through a unique modulatory action: GPR55 increases reluctant vesicles by depriving the sensitivity to APs, which is distinct from the mechanism suggested for CB1 receptor's effect.

Results

GPR55 inhibits synaptic transmission at PC output synapses

We first examined the role of GPR55 in synaptic transmission from a PC in acute cerebellar slices. Cerebellar sagittal slices were prepared from postnatal day (P)28-35 rats, and whole-cell patch-clamp recordings were performed from neurons with large cell bodies (> 15 μm diameter) in the DCN (Figure 1A; Uusisaari et al., 2006). The DCN neurons were voltage-clamped at -70 to -100 mV, and evoked IPSCs (eIPSCs) were recorded following electrical stimulation at the white matter in the presence of an AMPA receptor antagonist, NBQX (10 μM). In accord with previous studies (Kawaguchi and Sakaba, 2015), eIPSCs at PC-DCN synapses were identified by the sudden appearance of large amplitude responses (2.04 ± 0.48 nA) in an almost all-or-none manner as stimulation intensity was increased (Figure 1B). Bath application of a GPR55 agonist, AM251 (5 μM) decreased the amplitude of eIPSC (to 1.32 ± 0.35 nA, $p = 0.0278$, paired t-test), accompanied by an increase in the coefficient of variation (CV) of the responses (0.21 ± 0.03 to 0.39 ± 0.09, $p = 0.0394$, paired t-test) (Figure 1B, C). Increase of the CV is typically interpreted as a lowered presynaptic release probability. These results suggest that GPR55 suppresses synaptic transmission at PC-DCN synapses, similarly to what CB1 receptor does at other synapses (Kreitzer and Regehr, 2001; Ohno-Shosaku et al., 2001; Wilson and Nicoll, 2001; Diana et al., 2002). In order to validate the primary culture preparation, which allows a much more detailed analysis of synaptic function because of the feasibility to perform direct patch-clamp recordings from axon terminals, we also tested the action of GPR55 on PC outputs using the above-mentioned preparation. To fluorescently visualize PCs, we used an adeno-associated virus (AAV) vector, AAV2-CA-EGFP that preferentially infects PCs among neurons, as in previous studies (Kawaguchi and Sakaba, 2015). First, simultaneous whole-cell somatic patch-clamp recordings were performed from a presynaptic PC and its postsynaptic neuron (possible DCN neuron) surrounded by lots of EGFP-positive PC boutons, in the presence of NBQX (10 μM) (Figure 1D). Presynaptic PCs were voltage-clamped at -70 mV, and Na^+ current escaping as an AP from the patched soma to the axon was elicited by applying a voltage pulse (to 0 mV, 1~5 ms), which evoked IPSCs in the voltage-clamped postsynaptic target cell. In line with the data obtained in slices, synaptic transmission decreased upon GPR55 activation with AM251 (300 nM), manifested as a decrease in IPSC amplitude (from 591 ± 130 pA to 266 ± 27 pA, $p = 0.0374$, paired t-test) and an increase in the CV (from 0.57 ± 0.08 to 0.82 ± 0.07, $p = 0.0499$, paired t-test) (Figure 1E, F). A similar reduction in eIPSC amplitude and increase in its CV were observed with extracellular application of lysophosphatidylinositol (LPI, 1 μM), an endogenous ligand of GPR55 (amplitude: 457 ± 54 pA to 349 ± 68 pA, $p = 0.0118$, paired t-test; CV: 0.62 ± 0.07 to 0.71 ± 0.07, $p = 0.0341$, paired t-test) (Figure

1G, H). On the other hand, inhibition of GPR55 by an antagonist, CID16020046 (5 μM), abolished the suppressive effect of AM251 on synaptic transmission (amplitude: 566 ± 172 pA to 548 ± 128 pA, p = 0.998, paired t-test; CV: 0.44 ± 0.06 to 0.52 ± 0.07, p = 0.343, paired t-test) (Figure 1I, J). Neither application of AM251 nor LPI changed the time courses of IPSCs (20-80% risetime: 0.81 ± 0.06 ms to 0.77 ± 0.04 ms (AM251), p = 0.238, paired t-test; 0.71 ± 0.10 ms to 0.65 ± 0.12 ms (LPI), p = 0.318, paired t-test) (Figure S1A) and presynaptic Na^+ currents recorded at the PC soma (AM251: 3.30 ± 0.36 nA to 3.25 ± 0.44 nA, p = 0.419, paired t-test; LPI: 2.87 ± 0.30 nA to 2.89 ± 0.31 nA, p = 0.728, paired t-test) (Figure S1B, C). Taken together, these results suggest that GPR55 decreases neurotransmitter release at the synapses formed by PC axon terminals, acting presumably on the presynaptic side. It should be noted that AM251 is known to act not only as a GPR55 agonist, but also as a CB1 antagonist. However, taking it into consideration that PC synapses exhibit no modulation by CB1Rs (Hirono and Yanagawa, 2021), together with the fact that AM251 and LPI showed a similar depression, the effects of AM251 on synaptic outputs from a PC bouton were ascribed to activation of GPR55.

Recent studies suggested a possible site of action of GPR55 on hippocampal GABAergic synaptic transmission as the decreased accumulation of postsynaptic $GABA_A$ receptors (Khan A. et al., 2018; Rosenberg et al., 2023). On the other hand, the GPR55-mediated changes in the CV of eIPSCs amplitudes shown here at PC synapses suggest a presynaptic alteration. To obtain an insight into the site of AM251 action, miniature IPSCs (mIPSCs) were recorded from a possible cultured DCN cell innervated by lots of EGFP-labeled PC boutons in the presence of TTX (1 μM) and NBQX (10 μM) (Figure 1K and S2). As shown in Figure 1L and M, mIPSCs showed no change in amplitude or frequency after the AM251 application (amplitude: 54.3 ± 5.6 pA to 54.1 ± 4.9 pA, p = 0.944, paired t-test; frequency: 15.5 ± 0.9 Hz to 17.9 ± 2.3 Hz, p = 0.223, paired t-test). Thus, neither pre- nor postsynaptic sides exhibited a clear sign of functional changes in the AP-independent mIPSCs. Consequently, we hypothesized that the GPR55-dependent synaptic suppression is due to a decrease in the AP-triggered presynaptic Ca^{2+} influx via a reduced AP size and/or a negative regulation of presynaptic Ca^{2+} channels. These possibilities are explored in the following sections.

GPR55 suppresses transmitter release in PC boutons without changing presynaptic Ca^{2+} influx

As noted above, the decrease of synaptic transmission by GPR55 at presynaptic side would be possible if it affects an AP waveform or the resultant Ca^{2+} influx. Previous studies demonstrated that AP waveforms are subject to modulation in PC axons in a manner dependent on high frequency firing, local activation of axonal transmitter receptors, and/or intracellular cAMP changes (Kawaguchi and Sakaba, 2015; Zorrilla de San Martin et al., 2017; Furukawa et al., 2024). To test the possibility of a change in the AP waveform by GPR55, we performed direct patch-clamp recordings of APs from a presynaptic bouton of a PC axon (Figure 2A). As clearly shown in Figure 2B and C, neither the

amplitude nor the time course of the APs recorded in current-clamp at the axon terminals was modified by GPR55 activation with AM251 (amplitude: 91.1 ± 7.5 mV to 90.4 ± 6.4 mV, p = 0.701, paired t-test; half-width: 0.54 ± 0.06 ms to 0.54 ± 0.07 ms, p = 0.832, paired t-test). The next candidate as a potential site controlled by GPR55 is the presynaptic Ca^{2+} influx. A CB1-caused reduction of Ca^{2+} current has previously been shown by direct presynaptic recordings at the calyx of Held synapses and fluorescent imaging studies on the climbing fiber to PC synapses (Kreitzer and Regehr, 2001; Kushmerick et al., 2004; Wu et al., 2020). To record the presynaptic Ca^{2+} current, direct voltage-clamp recordings from PC boutons were performed. We also monitored the membrane capacitance (Cm) increase (ΔCm) caused by the Ca^{2+} influx, which is an indication of the amount of exocytosed synaptic vesicles. Unexpectedly, Ca^{2+} currents induced by square depolarizing pulses (0 mV for 5 ms) to the voltage-clamped PC boutons were not affected by AM251 (53 ± 6 pA/pF to 52 ± 6 pA/pF, p = 0.808, paired t-test), whereas the resultant increase of Cm was markedly diminished (21.9 ± 4.1 fF/pF to 12.9 ± 2.2 fF/pF, p = 0.0448, paired t-test) (Figure 2D, E). Thus, GPR55 does not modulate Ca^{2+} channels directly but still suppresses neurotransmitter release. Taken together, our direct patch-clamp recordings from PC terminals highlight a unique mechanism of GPR55-mediated downregulation of presynaptic function, that is distinct from the typical synaptic modulation by CB1 receptors, which depends on a reduction of presynaptic Ca^{2+} influx.

GPR55 decreases the amount of vesicles in the RRP

To obtain insights into the mechanism of GPR55-mediated suppression of neurotransmitter release, we biophysically analyzed the relation between presynaptic Ca^{2+} influx and vesicle exocytosis by systematically changing depolarization pulses to a PC bouton. Depolarizing pulses of different duration altered presynaptic Ca^{2+} current durations, leading to distinct amounts of vesicular release (Figure 3A). As summarized in Figure 3B, the Ca^{2+} current amplitude and its activation kinetics were again not significantly affected by the AM251-caused GPR55 activation at any depolarization duration (amplitude, p = 0.424; tau, p = 0.339, ANOVA), supporting the idea that GPR55 does not affect the presynaptic Ca^{2+} influx. On the other hand, ΔCm induced by any duration of depolarization pulses showed a ~50 % reduction in the presence of AM251 (29.8 ± 5.1 fF/pF and 14.8 ± 1.6 fF/pF upon 50 ms pulse without and with AM251, respectively, p = 0.0119, Student's t-test) (Figure 3C, D). Thus, GPR55 halves the amount of synaptic vesicles released within tens of milliseconds after a strong Ca^{2+} influx, corresponding to the readily-releasable pool (RRP), which could be the primary cause for the decrease in AP-triggered synaptic transmission.

Taking into consideration that the cytoplasm of PCs contains extremely potent Ca^{2+} buffering capacity due to the large amount of calbindin (Fierro and Llano, 1996; Bornschein et al., 2013), releasable vesicles in PC boutons might show a steep dependency of release competency on their position relative to the voltage-gated Ca^{2+} channels (VGCCs). Previous studies reported that vesicular fusion is insensitive to exogenous EGTA in the intracellular solution, a relatively slow but high-affinity

Ca^{2+} buffer, suggesting that vesicles that have the release machinery tightly coupled to VGCCs are release-competent in PC boutons (Kawaguchi and Sakaba, 2015; Diaz-Rojas et al., 2015). Accordingly, the RRP size was comparable between 0.5 mM and 5 mM cytoplasmic EGTA conditions without AM251 (0.5 mM EGTA: 29.8 ± 5.1 fF/pF; 5 mM EGTA: 35.7 ± 4.0 fF/pF upon 50 ms pulse, p = 0.385, Student's t-test) (Figure 3C and S3). On the other hand, previous studies showed decreased release by EGTA at synapses with relatively loose coupling between VGCCs and releasable vesicles, such as squid giant synapses, calyx of Held synapses, or hippocampal mossy fiber synapses (Adler et al., 1991; Borst and Sakmann, 1996; Vyleta and Jonas, 2014). Therefore, loosening the coupling between VGCCs and the release-competent vesicles by GPR55, if any, EGTA should be expected to become influential to the release even in PC boutons. However, the increase of cytoplasmic EGTA from 0.5 to 5 mM did not reduce the apparent RRP size in PC boutons even when GRP55 was activated by AM251 (5 mM EGTA: 19.1 ± 3.4 fF/pF upon 50 ms pulse with AM251, p = 0.488, compared to 0.5 mM EGTA with AM251 (14.8 ± 1.6 fF/pF), Student's t-test) (Figure 3C). Notably, plotting the fold reduction of ΔCm by AM251 against the duration of the depolarization suggested that a higher amount of EGTA made the suppressive effect of GPR55 stronger, particularly for the release in response to short pulses (Figure 3D). This result implies that the reduction of release by GPR55 might be somehow related to the Ca^{2+}-release coupling, although its extent is too small to be reflected as a clear change of release sensitivity to EGTA. In summary, based on biophysical analysis of Ca^{2+}-dependent release in terms of the modulations by AM251 and EGTA, we conclude that the GPR55 activation reduces the amount of vesicles in the RRP, which might be accompanied by a slight change of the functional coupling between release and Ca^{2+} influx.

Lowered and lagged vesicular fusion velocity by GPR55

To further investigate the GPR55-mediated downregulation of vesicular fusion, the Ca^{2+}-activated release kinetics were biophysically analyzed by simultaneous patch-clamp recordings from both a presynaptic PC bouton and a postsynaptic cell. To avoid saturation of postsynaptic $GABA_A$ receptors, we applied a short depolarization pulse (0 mV, 2 ms) to the patched bouton, and recorded presynaptic Ca^{2+} and postsynaptic currents (Figure 4A). Consistent with the above results, presynaptic Ca^{2+} current showed little change by the AM251 administration (42 ± 8 pA/pF to 44 ± 10 pA/pF, p = 0.348, paired t-test), while postsynaptic currents were clearly reduced by a half (2.57 ± 0.81 nA to 1.43 ± 0.52 nA, p = 0.0323, paired t-test) (Figure 4A, B). By deconvolving the postsynaptic currents with the template mIPSC trace, we estimated the temporal change of vesicular fusion velocity (for detail, see Methods; Kawaguchi and Sakaba, 2015). The peak of vesicular fusion velocity was almost halved by AM251 without a marked change of time course (45.7 ± 19.1 vesicles/ms to 25.7 ± 11.0 vesicles/ms, p=0.0308, paired t-test) (Figure 4C), showing similar reduction to that observed in the apparent RRP size (vesicular fusion velocity: 54.4 ± 8.4 %; ΔCm: 49.7 % upon 50 ms pulse shown

in Figure 3C). Thus, it would be reasonable to conclude that the RRP reduction, and not a change in the Ca^{2+}-activated release probability, predominantly underlies the synaptic suppression induced by GPR55. However, notably, the synaptic delay estimated by the time to the onset of release showed a tendency, although marginal, to increase after AM251 application (IPSC latency: 1.57 ± 0.39 ms to 1.98 ± 0.50 ms, p = 0.0441, paired t-test; onset of vesicular release: 1.63 ± 0.17 ms to 2.06 ± 0.28 ms, p = 0.0260, paired t-test) (Figure 4C). Thus, together with the idea that GPR55 somehow lowers the effectiveness of Ca^{2+}-triggered release (as shown in Figure 3D), the apparent RRP reduction by GPR55 in PC boutons might also be caused by a process accompanied with a slight lowered velocity of the Ca^{2+}-mediated activation process of vesicular fusion.

Reduction of AP-sensitive vesicles by GPR55

The above experiments demonstrated that GPR55 reduces synaptic transmission primarily by reducing the RRP size without altering Ca^{2+} influx at the presynaptic terminal. To discriminate two possible causes for the decrease in RRP size: relative increase in the fraction of reluctant vesicles or reduction in the number of total vesicles present at the presynaptic terminal, we performed fluorescence imaging of vesicular fusion with synapto-pHluorin expressed in PCs using AAV or microinjection of DNA plasmid into the nucleus. First, APs were repetitively evoked (400 APs at 20 Hz) at the voltage-clamped PC soma by depolarization pulses triggering somatic Na^{+} currents (Figure S4), and the fluorescence changes of pHluorin at axon terminals were monitored. Synapto-pHluorin shows little fluorescence upon light illumination when its pH-sensitive fluorophore is exposed to the acidic vesicular lumen, and becomes fluorescent after exocytosis through the exposure to the external neutral pH environment (Figure 5A), providing the sign of vesicle fusion as a fluorescence increase (Sankaranarayanan et al., 2000; Sankaranarayanan and Ryan, 2000). As shown in Figure 5B-D, synapto-pHluorin imaging showed fluorescence increase at PC axonal varicosities by 23.4 ± 2.1 % upon 400 APs. After the increase of fluorescence during the AP train stimulation, pHluorin signal decayed with a time constant of about 40 sec, reflecting the endocytosis of exocytosed synapto-pHluorin and the subsequent re-acidification of the vesicular lumen (Nicholson-Tomishima and Ryan, 2004; Yamashita et al., 2018). Consistently with the GPR55-mediated reduction of synaptic transmission (see Figure 1), AM251 administration reduced the pHluorin signal increase evoked by the 400 APs (ΔF_{400APs}) by 50.6 ± 4.7 % in average (p = 9.12e-7), with no change in its decay time course (τ_{decay}: 42.1 ± 7.8 sec to 40.9 ± 4.5 sec, p = 0.780, paired t-test) (Figure 5C). The AP-triggered increase of pHluorin fluorescence was specific to axonal varicosities, and the GPR55 activation simply reduced the size of the fluorescence increase (Figure 5B-D). Interestingly, however, plotting the extent of release reduction by AM251 against the original size of ΔF_{400APs} indicated that boutons showing a larger amount of release tend to be more susceptible to suppression by the GPR55 activation (Figure 5E). This indicates that the variable control of the synaptic output exerted by GPR55 depends on the

original amount of release in individual boutons along a PC axon. On the other hand, when the intracellular vesicles with an acidic internal lumen were ubiquitously neutralized by exogenous application of NH_4Cl (50 mM), as depicted in Figure 5A, pHluorin fluorescence increased by 347.0 ± 5.1 % in the control condition and 330.3 ± 11.1 % in the presence of AM251 ($p = 0.632$, Student's t-test) (Figure 5F, G), indicating that the total amount of vesicles at individual boutons is similar in both conditions. It should be noted that ΔF_{400APs} by itself exhibited a large variability across boutons, showing a linear relation to the 2/3th power (for calibration between volume and surface area of boutons) of that by NH_4Cl (ΔF_{NH4Cl}) (Figure 5H). Thus, the original fraction of released vesicles in response to APs seemed constant in average among distinct boutons; in larger boutons containing more vesicles the ΔF_{400APs} is simply higher. In addition, the predicted distribution pattern of ΔF_{400APs} with GPR55 activation calculated from the relation between the extent of GPR55-mediated release reduction and the ΔF_{400APs} (shown in Figure 5E) nicely overlapped the actual data obtained after the AM251 application (Figure 5H). Thus, the fluorescent live imaging of AP-triggered vesicle fusion revealed that the GPR55 reduces vesicular fusion in response to APs, without changing the total amount of vesicles present at individual PC boutons.

To obtain further insights into the dynamics of synaptic vesicular pools possibly affected by GPR55, such as transitions among the readily-releasable, recycling, reserve, and release-reluctant pools at individual boutons (Fernandez-Alfonso and Ryan, 2008; Kim and Ryan, 2010; Cazares et al., 2016; Mori et al., 2021), we repeatedly induced the 400 APs firing at the soma and measured the size of the fluorescence increase at boutons before and after the suppression of re-acidification of endocytosed vesicles with bafilomycin (100 nM), an inhibitor of vesicular ATPase (Sankaranarayanan and Ryan, 2000). As shown in Figure 6A (black trace), bafilomycin application enhanced the ΔF_{400APs} (by 56.0 ± 9.9 %, $p = 2.32e-4$), and abolished the fluorescence decay after the end of the stimulation (relative ΔF_{400APs} remaining at 20s after the end of APs: 52.6 ± 6.5 % (control) to 97.0 ± 5.1 % (bafilomycin), $p =0.0004$, paired t-test), reflecting the inhibition of the re-acidification of endocytosed vesicles, which takes place in naïve conditions during the stimulation and lasts tens of seconds after it. Repeating the 400 APs stimulations after the bafilomycin application resulted in additive fluorescence increase, eventually reaching a plateau at 27.6 ± 2.7 % of the maximal fluorescence increase upon the NH_4Cl application (Figure 6A). This suggests that synaptic vesicles corresponding to those for ~1000 APs are totally release-competent at individual axon terminals, in accord with previous studies (Kawaguchi and Sakaba, 2015). In order to induce the exocytosis of the remaining releasable vesicles in the terminal, if any, after the 7 sets of 400 APs train stimulation, KCl (50 mM) was added to the external bath to potently depolarize the plasma membrane. In these conditions, little further increase in the pHluorin signal was observed (Figure 6A), confirming that most depolarization-sensitive vesicles have undergone fusion during the AP trains.

Intriguingly, the reduction of the ΔF_{400APs} by AM251 (red trace in Figure 6A) was evident throughout the 400 APs train stimulations (~10 minutes total time), reaching a plateau of about 13.7 ± 1.6 % of the total amount of vesicles (Figure 6A, p = 3.36e-4 compared with control (27.6 ± 2.7 %), Student's t-test). This implies that the total amount of releasable vesicles upon repeated APs for minutes, which is composed by the RRP, the recycling pool and even some reserve pool of vesicles, gets smaller in number when GPR55 is activated. To further obtain insight into the reduced releasable vesicles by GPR55, we triggered vesicular release from PC boutons by causing an aberrant cytoplasmic Ca^{2+} increase by adding ionomycin, which induces the formation of Ca^{2+}-conducting pores on the plasma membrane. Surprisingly, application of ionomycin (10 μM) increased pHluorin signal to almost identical levels irrespective of the presence of AM251 (54.2 ± 1.1 % and 57.6 ± 1.9 % of total vesicles without and with AM251, respectively, p = 0.104, Student's t-test) (Figure 6B). When comparing the cytoplasmic Ca^{2+} increases in response to APs with those in response to ionomycin, monitored by GCaMP7f fluorescence imaging, ionomycin induced a much more potent and broader Ca^{2+} increase throughout PC axons than the Ca^{2+} increase induced by the inflow through VGCCs upon APs stimulation (Figures 6C-F; $\Delta F/F$ upon 400 APs and ionomycin: varicosity, 7.02 ± 0.36 of and 16.46 ± 0.69, p = 2.13e-19 by paired t-test; axon, 1.45 ± 0.18 and 15.1 ± 1.30, p = 6.42e-11 by paired t-test). It should be noted that the size of the vesicle pool which underwent fusion upon ionomycin application was almost double of the pool which underwent exocytosis upon thousands of APs. Thus, only half of Ca^{2+}-responsive releasable vesicles may be sensitive to APs in the naïve PC axonal terminals, which is further reduced when GPR55 is activated.

Discussion

In this study we used a combination of subcellular patch-clamp recordings from axon terminals and fluorescence imaging of presynaptic vesicular exocytosis in cerebellar primary cultures, together with electrophysiology in cerebellar slices, in order to demonstrate that synaptic transmission is suppressed by activation of GPR55, a type of cannabinoid receptor. The mechanism of action involves a transformation of the presynaptic vesicles, which become insensitive to APs, while the Ca^{2+} influx is kept constant in the terminal. Thus, a unique mechanism to negatively control synaptic outputs is unveiled here, which would provide a way to fine-tune the neuronal computation in the brain in coordination with the typical modulation of synaptic efficacy by conventional cannabinoid receptors.

Modulation of synaptic function by endocannabinoids

Later than findings of critical roles of CB1 receptor in fine tuning of neuronal circuit function, another type of cannabinoid receptor, GPR55 was identified (Baker et al., 2006; Oka et al., 2007). GPR55 seems to be activated by 2-AG and annandamid, as CB1/CB2 receptor, although the

downstream signaling is different, and also shows affinity to cannabidiol, another molecule found in cannabis (Henstridge et al., 2008; Oka et al., 2009). Distinct from typical chemical components of cannabis such as tetrahydrocannabinol (THC), interestingly, cannabidiol has been shown to modulate the function of nervous system with limited addictive power, and thus have attracted attention for possible therapeutic applications for mental disorders (Denis et al., 2024). Thus, the physiological actions of GPR55 are now increasingly studied, although its detailed effect on neuronal computation still remains largely veiled. Recently, GPR55 was shown to modulate synaptic transmission efficacy at both excitatory and inhibitory synapses in the hippocampus through augmentation of presynaptic release probability and modulation of postsynaptic $GABA_A$ receptors, respectively (Rosenberg et al., 2023). In contrast, our data showed no detectable changes in mIPSC amplitudes by GPR55 in potential DCN neurons (see Figure 1L, M). Thus, the modulation of $GABA_A$ receptors by GPR55 might be subtype- and/or neuronal type-specific. Rather, here we observed a remarkable suppression of presynaptic function by GPR55 through a change in the releasable vesicle amounts and/or properties in PC terminals. Considering the endogenous ligands for GPR55 such as LPI, which are produced upon activation of phospholipase A1 and A2, the GPR55-mediated modulation of synaptic function revealed here might provide another efficient way to control the circuit function depending on the specific types of endocannabinoids and the receptors involved. It is an important issue to be clarified in the future what neuronal situation leads to the production of endogenous GPR55 ligands like LPI, and how the synapses are modulated in terms of strength and time course.

One extensively studied activity-dependent short-term depression of synaptic strength in the CNS is DSE and/or DSI, which are typically caused by a strong postsynaptic depolarization accompanied with potent Ca^{2+} increases or the G_q-coupled metabotropic receptors such as group-I mGluRs, activating PLC and/or diacylglycerol lipase. Both enzymes produce typical endocannabinoids such as 2-AG and annandamide, which then reach retrogradely on presynaptic boutons beyond plasma membranes and synaptic cleft (Kano et al., 2009; Castillo et al., 2012). As a result, CB1 receptor located at the presynaptic membrane is activated and then Ca^{2+}-triggered transmitter release is suppressed for tens of seconds (Kreitzer and Regehr, 2001; Ohno-Shosaku et al., 2001; Wilson and Nicoll, 2001; Diana et al., 2002). Such short-term forms of presynaptic plasticity have been found to take place at a variety of synapses in the CNS including the hippocampus, cerebellum, prefrontal cortex, amygdala, and so on (Kano et al., 2009; Di Marzo et al., 2001; Katona 2001; Hill and Patel, 2013), which has provided basic knowledge about the primary mechanisms of cannabis intake into brain computation. In addition, CB1 receptor has been shown to play roles in long-term synaptic plasticity and hence learning and memory in animals (Kano et al., 2009; Gómez-Gonzalo et al., 2015). On the other hand, the functional role of another cannabinoid receptor CB2 has been largely unknown. CB2 receptor exogenously expressed in hippocampal autaptic neurons from CB1 null mice was shown to suppress synaptic transmission and restore DSE (Atwood et al., 2012). In contrast, in spite of CB2 being expressed in PCs (Ashton et al., 2006), no modulation of synaptic

outputs from PC axons has been demonstrated (Hirono and Yanagawa, 2021). Thus, as demonstrated here, PC axon terminals might be equipped with a compensatory mechanism to control outputs through GPR55 in place of CB2 receptor.

Mechanisms for synaptic modulations by GPR55 distinct from CB1/CB2 receptors

Unlike typical metabotropic receptors, here we have shown that GPR55 reduces vesicular exocytosis by making the Ca^{2+}-sensitive release-competent vesicles reluctant upon AP arrival without changing the Ca^{2+} influx and vesicular Ca^{2+} responsiveness (see Figure 3-6). GPR55 is coupled to $G_{12/13}$-type of G protein, which activates small G protein signaling such as cdc42, Rac and RhoA (Ryberg et al., 2007), and is known to change actin cytoskeleton (Harada et al., 2017). Rapid replenishment and/or endocytosis of synaptic vesicles are known to depend on actin dynamics (Lee et al., 2012; Miki et al., 2016), which might be related to the altered vesicular sensitivity to Ca^{2+} influx through VGCCs after the GRP55 activation. In any case, the unique control of presynaptic function by $G\alpha_{12/13}$-coupled GRP55 demonstrated here would provide a complementary modulation of synaptic outputs by cannabinoids together with CB1/CB2 receptor, and the detailed molecular mechanism is an important issue to be clarified in the future.

On the other hand, previous studies have clarified the molecular mechanisms by which CB1 receptor exerts a negative modulation of synaptic transmission. As well as a typical inhibitory modulation by metabotropic receptors such as group2 metabotropic glutamate receptors and $GABA_B$ receptors (Kew et al., 2001; Takahashi et al., 1998; Bowery et al., 2002), CB1 and CB2 receptors are thought to couple to $G_{i/o}$-type of trimeric G-protein, negatively regulating the activation and/or conductance of VGCCs (Guo and Ikeda, 2004). Taking into consideration that the vesicular exocytosis steeply depends on the local Ca^{2+} concentration around the Ca^{2+} sensor synaptotagmin (Schneggenburger and Neher, 2000), the reduction of Ca^{2+} influx is enough to explain the suppression of transmitter release.

Dynamics of synaptic vesicles among distinct functional pools

Inspired by the GPR55-mediated marked decrease of RRP vesicles demonstrated here by the presynaptic Cm measurement and biophysical analysis, we live-imaged vesicular fusion with synapto-pHluorin to functionally dissect the altered pools of vesicles in PC terminals (see Figures 5, 6). Surprisingly, the reduced releasable fraction upon GPR55 activation was only evident when release was triggered by APs, but undetectable in response to ionomycin, indicating that the apparent RRP reduction would be highly related to the source of cytoplasmic Ca^{2+} increase. Taking into consideration that the RRP reduction was also evident when the Ca^{2+} increase was triggered by much stronger stimulation (50 ms direct presynaptic depolarization), the discrepancy between the effects of GPR55 on the release caused by the presynaptic depolarization and the Ca^{2+} ionophore could be reasonably ascribed to the relationship between the release sites and Ca^{2+} sources. Notably, our

imaging experiments indicated that the total recycling pool of vesicles which underwent exocytosis by thousands of APs during ~10 minutes corresponds to only ~25 % of total vesicles, that is, a half of Ca^{2+}-sensitive release-competent vesicles that could fuse upon aberrant Ca^{2+} increase via the Ca^{2+}-conducting ionophore (see Figure 6B, C). Because of the extremely potent and rapid Ca^{2+} buffering system in the cytoplasm of PCs due to the abundant expression of calbindin (Fierro and Llano, 1996), the Ca^{2+} influx from VGCCs is expected to activate vesicles with the Ca^{2+} sensor very close to VGCCs. Thus, it is implied that the release-competent vesicles relatively far from VGCCs may stay at their position for minutes without being exocytosed or getting into the AP-sensitive pools. Indeed, it was shown that the relatively large increase in cytoplasmic Ca^{2+} concentration by activating IP_3-caused release from the internal Ca^{2+} store in PC terminals, is only effective for the AP-independent spontaneous vesicular releases detected as miniature postsynaptic responses (Gomez et al., 2020). Thus, at least in PCs, which are equipped with a very strong Ca^{2+} buffering system, the functional categorization of depolarization-sensitive vesicles seems to be influenced by the physical distance of vesicles and the source of Ca^{2+}. Interestingly, the reduction of releasable vesicles by GPR55 activation is limited to the AP-sensitive ones among Ca^{2+}-sensitive ones (see Figure 6). Thus, taking the two findings together into consideration that GPR55 suppresses more potently the release caused by smaller Ca^{2+} influx in the presence of high EGTA (see Figure 3) and delays the onset of release (see Figure 4), it would be reasonable to presume that the functional coupling between VGCCs and release machinery is loosened by the GPR55 activation. The loosened Ca^{2+}-release coupling, if any, upon GPR55 activation operating as the mechanism for synaptic suppression would compromise with the lack of changes in frequency of mIPSCs (see Figure 1). The fact that GPR55 activation leads to altered actin cytoskeleton organization also makes this scenario plausible. Previously, it was shown that the releasable vesicle pool is altered by cdk5 and/or Tomosyn1 in hippocampal neurons (Kim and Ryan, 2010; Cazares et al., 2016). Recent direct patch-clamp recordings combined with super-resolution fluorescence or electron microscopic imaging are highlighting the dynamic change of the Ca^{2+}-release coupling distance (Fukaya et al., 2021; Midorikawa et al., 2024). The exact change of release machinery relative to VGCCs at high resolution as ~ nm in PC boutons upon GPR55 activation is a critical issue to be clarified in the future.

Materials and Methods

Animal usage

All experimental procedures were performed in accordance with regulations on animal experimentation in Kyoto University and approved by the local committee in Graduate School of Science, Kyoto University. Wistar rats (Slc: Wistar; Japan Slc Inc., Hamamatsu, Japan) of either sex were used in this study. Rats were housed with a mother rat until weaning in filter-top cages with bedding at 20−24°C under a 12/12 h light/dark photocycle. Food and water were available *ad libitum*. Rats at P0–16 were killed by decapitation, and older ones by anaesthetization with isoflurane in air, then decapitation.

Slice preparation

Acute sagittal slices (200 μm thickness) of cerebellum were prepared from Wistar rats at P28-42 for experiments with AM251. Rats were anesthetized with isoflurane and perfused transcardially with ice-cold sucrose solution containing the following (in mM): NaCl 60, sucrose 120, $NaHCO_3$ 25, NaH_2PO_4 1.25, KCl 2.5, D-glucose 25, ascorbic acid 0.4, myo-inositol 3, Na-pyruvate 2, $CaCl_2$ 0.1, $MgCl_2$ 3, pH 7.3-7.4, 300-350 mOsm/Kg H_2O with continuous bubbling with mixed gas (95% O_2 and 5% CO_2). After decapitation, the cerebellum was quickly removed and cut with a Leica vibroslicer (VT1200S) in an ice-cold K-Gluconate-based solution (for P28-P35 rats) containing the following (in mM): K-Gluconate 130, KCl 15, EGTA (ethylene glycol-bis(β-aminoethyl ether)-N,N,N′,N′-tetraacetic acid) 0.05, HEPES (4-(2-hydroxyethyl)-1-piperazineethanesulfonic acid) 20, glucose 25, and D-AP5 50 μM, pH 7.4, 300-350 mOsm/Kg H_2O, with continuous bubbling with mixed gas (95% O_2 and 5% CO_2). Slices were then incubated at 37 °C for a half to 1 h in an extracellular solution containing the following (in mM): NaCl 125, $NaHCO_3$ 25, NaH_2PO_4 1.25, KCl 2.5, D-glucose 25, ascorbic acid 0.4, myo-inositol 3, Na-pyruvate 2, $CaCl_2$ 2, $MgCl_2$ 1, pH 7.3-7.4, 300-320 mOsm/Kg H_2O with continuous bubbling with mixed gas.

Cerebellar primary cultures

The method for preparing primary dissociated cultures of cerebellar neurons was similar to that in previous studies (Kawaguchi and Hirano, 2007). Briefly, cerebella were dissected out from newborn rats and their meninges were removed. The cerebella were incubated in Ca^{2+} and Mg^{2+}-free Hank's balanced salt solution containing 0.1% trypsin and 0.05% DNase for 15 min at 37°C. Cells were dissociated by trituration and seeded in Dulbecco's modified Eagle's medium: nutrient mixture F12-based medium containing 2% fetal bovine serum. On the next day, ~ 80% of medium was replaced by basal medium Eagle. After that, half of the medium was changed every 3−4 days. Cytosine arabinoside (4 μM) was added to the medium to inhibit proliferation of glial cells. PCs could be visually identified by large cell bodies and thick dendrites. Experiments were performed >21 days after

preparation of the culture.

DNA construction and transfection

Plasmids containing coding DNA sequences of synapto-pHluorin, EGFP, Venus, GCaMP7f were the same as previous studies (Kawaguchi and Hirano, 2007; Kawaguchi and Sakaba, 2015; Higashi et al., 2024). DNA fragments for tTA and TRE sequences were obtained from Tet-off system (Clonetech). cDNAs were inserted into the pAAV-CA-WPRE plasmid (Higashi et al., 2024). PCs were transfected at 4-7 days after culture with an AAV vector serotype 2. For some imaging experiments using synapto-pHluorin, the DNA expression plasmid encoding synapto-pHluorin was directly injected into the nucleus of a PC through a sharp glass pipette (Kawaguchi and Hirano, 2007). The electrophysiological or immunocytochemical experiments were performed 1–2 days after the injection.

Electrophysiology

Patch-clamp recording was performed with an amplifier (EPC10, HEKA, Stuttgart, Germany) at room temperature (20-24 °C), in an extracellular solution mentioned above for slices, or that containing the following for culture (in mM): NaCl 145, HEPES 10, glucose 10, $CaCl_2$ 2, $MgCl_2$ 1, pH 7.3-7.4 adjusted by KOH, and 300-310 mOsm/Kg H_2O, using an inverted IX71 microscope (Olympus, Tokyo, Japan) equipped with a 40×, 0.95 numerical aperture (NA) objective or an upright BX51WI (Olympus) equipped with a 60×, 1.0 NA objective. Images were obtained with a Zyla4.2 sCMOS camera (Andor; Oxford Instruments, Oxford, UK). In some experiments, 2,3-Dioxo-6-nitro-1,2,3,4-tetrahydrobenzo[f]quinoxaline-7-sulfonamide (NBQX, 10 μM), tetrodotoxin (TTX, 1 μM) and tetraethylammonium (TEA, 2 mM) were applied to the bath. For current-clamp recordings, KCl-based internal solution with the following composition (in mM) was used: KCl 147, HEPES 10, EGTA 0.5, Mg-ATP 2, Na-GTP 0.2, pH 7.3-7.4 adjusted by KOH, and 320-330 mOsm/Kg H_2O. For voltage clamp recordings from PC-target neurons, a patch pipette was filled with a CsCl-based internal solution (pH 7.3-7.4 adjusted by CsOH and 320-330 mOsm/Kg H_2O) containing (in mM): CsCl 147, HEPES 10, EGTA 0.5, Mg-ATP 2, Na-GTP 0.2. For voltage-clamp recordings from PC axon terminals, the internal solution was composed of (in mM): CsCl 103, KCl 44, HEPES 10, EGTA 5, Mg-ATP 2, Na-GTP 0.2 (pH 7.3-7.4 adjusted by CsOH and 320-330 mOsm/KgH_2O), and recordings were performed in the presence of external TTX (1 μM) and TEA (2 mM). AM251 (5 μM for slice or 500 nM for culture), LPI (1 μM), CID16020046 (5 μM) or WIN 55,212-2 (500 nM) were applied to the bath. Membrane potential of a PC was held at -70 mV unless otherwise stated. PCs' target postsynaptic neurons were voltage clamped at -70 to -100 mV in slices, or at -70 mV in culture for IPSC recordings to avoid unclamped Na^+ currents. Series resistances in recordings from the PC soma and presynaptic bouton were 15 ± 5 MΩ and 142 ± 52 MΩ (mean ± SEM; n = 44 and 55 cells, respectively). On-line series resistance compensation (20-60%) was applied for IPSC recordings, and the remaining resistance was corrected

off-line after the recording. In paired whole-cell recordings from a presynaptic PC soma and its postsynaptic neuron, APs were elicited by voltage pulses to 0 mV for 1 ~ 5 ms into PC soma. In the slice, IPSCs were evoked by a glass pipette placed in the white matter. The onset of release was defined as the first time point at which the recorded current value showed change larger than 2 SDs of that at the basal condition. Average amplitude and frequency of mIPSCs for individual cells were calculated from ≥ 200 events, showing ≥ 7 pA amplitude and appropriate time courses.

Measuring of Cm was done using sine +DC technique (Neher and Marty, 1982) implemented on the PatchMaster software (HEKA, Germany). Presynaptic terminals were held at -80 mV and the sine wave (1 kHz and the peak amplitude of 30 mV) was applied on the holding potential. Because membrane conductance fluctuates during the depolarizing pulse, Cm was usually measured between around 50 ms after the depolarization. To estimate the clamped area in a direct bouton recording, capacitive transients in response to a hyperpolarizing pulse (5 or 10 mV) were used. Capacitive transients at a bouton followed a single exponential with time constants of 0.38 ± 0.02 ms (n = 55 cells), so that the clamped terminal size was estimated to be 2.7 ± 0.2 pF on average. To normalize the variation in Ca^{2+} currents and neurotransmitter release depending on the size of the bouton, presynaptic Ca^{2+} current and Cm were normalized by the Cm under the voltage-clamp in each bouton (in Figure 2 - 6).

Fluorescence imaging of pHluorin or GCaMP

Fluorescence imaging was performed using an upright microscope BX51WI (Olympus) through a 60× 1.0-NA objective (Olympus). Fluorescent excitation was delivered using an LED (M470L4, Thorlabs). Images of pHluorin or GCaMP7f fluorescence in PC axon terminals were obtained at 0.5 Hz with Zyla4.2 sCMOS camera (Andor), and analyzed with SOLIS (Andor) or ImageJ (NIH). APs were evoked at the voltage-clamped PC soma by depolarization (0 mV, 5 ms). Bafilomycin (100 nM), ionomycin (10 μM), KCl (50 mM) or NH_4Cl (50 mM) were applied to the bath.

Statistics

Data are presented as mean ± SEM unless otherwise stated. Statistical significance was evaluated by paired t-test, unpaired Students' t-test for unpaired groups, one-way ANOVA or two-way ANOVA for multiple comparison. Statistical significance was considered to be $p < 0.05$.

Acknowledgments

We thank Drs Mitsuharu Midorikawa and Federico Trigo for the critical reading of the manuscript and helpful comments.

Competing interests

The authors declare no competing interests.

Funding

Japan Society for Promotion of Science, KAKENHI grants 22H02721 (SK), 22K19360 (SK), 24K18217(TI) and 21K15189(TI). Takeda Science Foundation (SK). Naito Foundation (SK).

Reference

1. Abbott LF, Regehr WG. (2004) **Synaptic computation** *Nature* **431**:796-803. DOI: https://doi.org/10.1038/nature03010, PMID: 15483601
2. Adler EM, Augustine GJ, Duffy SN, Charlton MP. (1991) **Alien intracellular calcium chelators attenuate neurotransmitter release at the squid giant synapse** *The Journal of Neuroscience* **11**:1496–1507. DOI: https://doi.org/10.1523/JNEUROSCI.11-06-01496.1991, PMID: 1675264
3. Ashton JC, Friberg D, Darlington CL, Smith PF. (2006) **Expression of the cannabinoid CB2 receptor in the rat cerebellum: an immunohistochemical study** *Neuroscience Letters* **396**:113-116. DOI: https://doi.org/10.1016/j.neulet.2005.11.038, PMID: 16356641
4. Atwood BK, Straiker A, MacKie K. (2012) **CB_2 cannabinoid receptors inhibit synaptic transmission when expressed in cultured autaptic neurons** *Neuropharmacology* **63**:514–523. DOI: https://doi.org/10.1016/j.neuropharm.2012.04.024, PMID: 22579668
5. Baker D, Pryce G, Davies WL, Hiley CR. (2006) **In silico patent searching reveals a new cannabinoid receptor** *Trends in Pharmacological Sciences* **27**:1–4. DOI: https://doi.org/10.1016/j.tips.2005.11.003, PMID: 16318877
6. Bornschein G, Arendt O, Hallermann S, Brachtendorf S, Eilers J, Schmidt H. (2013) **Paired-pulse facilitation at recurrent Purkinje neuron synapses is independent of calbindin and parvalbumin during high-frequency activation** *The Journal of Physiology* **591**:3355-3370. DOI: https://doi.org/10.1113/jphysiol.2013.254128, PMID: 23671160
7. Borst JG, Sakmann B. (1996) **Calcium influx and transmitter release in a fast CNS synapse** *Nature* **383**:431–434. DOI: https://doi.org/10.1038/383431a0, PMID: 8837774
8. Bowery NG, Bettler B, Froestl W, Gallagher JP, Marshall F, Raiteri M, Bonner TI, Enna SJ. (2002) **International Union of Pharmacology. XXXIII. Mammalian gamma-aminobutyric acid(B) receptors: structure and function** *Pharmacological Reviews* **54**:247-264. DOI: https://doi.org/10.1124/pr.54.2.247, PMID: 12037141
9. Castillo PE, Younts TJ, Chávez AE, Hashimotodani Y. (2012) **Endocannabinoid signaling and synaptic function** *Neuron* **76**:70-81. DOI: https://doi.org/10.1016/j.neuron.2012.09.020, PMID: 23040807
10. Cazares VA, Njus MM, Manly A, Saldate JJ, Subramani A, Ben-Simon Y, Sutton MA, Ashery U, Stuenkel EL. (2016) **Dynamic Partitioning of Synaptic Vesicle Pools by the SNARE-Binding Protein Tomosyn** *The Journal of Neuroscience* **36**:11208-11222. DOI: https://doi.org/10.1523/JNEUROSCI.1297-16.2016, PMID: 27807164
11. Denis Völker JS, Micluția IV, Vinași RC. (2024) **Investigating Cannabidiol's potential as a supplementary treatment for schizophrenia: A narrative review** *European Journal of Pharmacology* **979**:176821. DOI: 10.1016/j.ejphar.2024.176821, PMID: 39068976
12. Devinsky O, Jones NA, Cunningham MO, Jayasekera BAP, Devore S, Whalley BJ. (2024) **Cannabinoid treatments in epilepsy and seizure disorders** *Physiological Reviews* **104**:591-649. DOI: https://doi.org/10.1152/physrev.00049.2021, PMID: 37882730
13. Di Marzo V, Goparaju SK, Wang L, Liu J, Bátkai S, Járai Z, Fezza F, Miura GI, Palmiter RD, Sugiura T, Kunos G. (2001) **Leptin-regulated endocannabinoids are involved in maintaining food intake** *Nature* **410**:822-825. DOI: https://doi.org/10.1038/35071088, PMID: 11298451
14. Diana MA, Levenes C, Mackie K, Marty A. (2002) **Short-term retrograde inhibition of GABAergic synaptic currents in rat Purkinje cells is mediated by endogenous cannabinoids** *The Journal of Neuroscience* **22**:200-208. DOI: https://doi.org/10.1523/JNEUROSCI.22-01-00200.2002, PMID: 11756503
15. Díaz-Rojas F, Sakaba T, Kawaguchi SY. (2015) **Ca^{2+} current facilitation determines short-term facilitation at inhibitory synapses between cerebellar Purkinje cells** *The Journal of Physiology* **593**:4889–4904. DOI: https://doi.org/10.1113/JP270704, PMID: 26337248
16. Fernandez-Alfonso T, Ryan TA. (2008) **A heterogeneous "resting" pool of synaptic vesicles that is dynamically interchanged across boutons in mammalian CNS synapses** *Brain Cell Biology* **36**:87-100. DOI: https://doi.org/10.1007/s11068-008-9030-y, PMID: 18941900
17. Fierro L, Llano I. (1996) **High endogenous calcium buffering in Purkinje cells from rat cerebellar slices** *The Journal of Physiology* **496**:617-625. DOI: https://doi.org/10.1113/jphysiol.1996.sp021713, PMID: 8930830
18. Fukaya R, Maglione M, Sigrist SJ, Sakaba T. (2021) **Rapid Ca^{2+} channel accumulation contributes to cAMP-mediated increase in transmission at hippocampal mossy fiber**

synapses *PNAS* **118**:e2016754118. DOI: 10.1073/pnas.2016754118, PMID: 33622791
19. Furukawa K, Inoshita T, Kawaguchi SY. (2024) **Graded control of Purkinje cell outputs by cAMP through opposing actions on axonal action potential and transmitter release** *The Journal of Physiology* DOI: https://doi.org/10.1113/JP286668, PMID: 39052311
20. Gómez-Gonzalo M, Navarrete M, Perea G, Covelo A, Martín-Fernández M, Shigemoto R, Luján R, Araque A. (2015) **Endocannabinoids Induce Lateral Long-Term Potentiation of Transmitter Release by Stimulation of Gliotransmission** *Cerebral Cortex* **25**:3699-3712. DOI: https://doi.org/10.1093/cercor/bhu231, PMID: 25260706
21. Gomez LC, Kawaguchi SY, Collin T, Jalil A, Gomez MDP, Nasi E, Marty A, Llano I. (2020) **Influence of spatially segregated IP3-producing pathways on spike generation and transmitter release in Purkinje cell axons** *PNAS* **117**:11097-11108. DOI: https://doi.org/10.1073/pnas.2000148117, PMID: 32358199
22. Guo J, Ikeda SR. (2004) **Endocannabinoids modulate N-type calcium channels and G-protein-coupled inwardly rectifying potassium channels via CB1 cannabinoid receptors heterologously expressed in mammalian neurons** *Molecular Pharmacology* **65**:665-674. DOI: https://doi.org/10.1124/mol.65.3.665, PMID: 14978245
23. Harada K, Kitaguchi T, Kamiya T, Aung KH, Nakamura K, Ohta K, Tsuboi T. (2017) **Lysophosphatidylinositol-induced activation of the cation channel TRPV2 triggers glucagon-like peptide-1 secretion in enteroendocrine L cells** *The Journal of Biochemistry* **292**:10855-10864. DOI: https://doi.org/10.1074/jbc.M117.788653, PMID: 28533434
24. Henstridge CM, Balenga NA, Ford LA, Ross RA, Waldhoer M, Irving AJ. (2008) **The GPR55 ligand L-alpha-lysophosphatidylinositol promotes RhoA-dependent Ca^{2+} signaling and NFAT activation** *The FASEB Journal* **23**:183-193. DOI: https://doi.org/10.1096/fj.08-108670, PMID: 18757503
25. Higashi R, Morita M, Kawaguchi SY. (2024) **Cl^--dependent amplification of excitatory synaptic potentials at distal dendrites revealed by voltage imaging** *Science Advances* **10**:eadj2547. DOI: https://doi.org/10.1126/sciadv.adj2547, PMID: 39196927
26. Hill MN, Patel S. (2013) **Translational evidence for the involvement of the endocannabinoid system in stress-related psychiatric illnesses** *Biology of Mood & Anxiety Disorders* **3**:19. DOI: https://doi.org/10.1186/2045-5380-3-19, PMID: 24286185
27. Hirono M, Yanagawa Y. (2021) **Endocannabinoids regulate cerebellar GABAergic transmission in a synapse type-dependent manner** *Journal of Neuroscience Research* **99**:898–913. DOI: https://doi.org/10.1002/jnr.24765, PMID: 33271631
28. Kandel ER. (2001) **The molecular biology of memory storage: a dialogue between genes and synapses** *Science* **294**:1030-1038. DOI: https://doi.org/10.1126/science.1067020, PMID: 11691980
29. Kano M, Ohno-Shosaku T, Hashimotodani Y, Uchigashima M, Watanabe M. (2009) **Endocannabinoid-mediated control of synaptic transmission** *Physiological Reviews* **89**:309-380. DOI: https://doi.org/10.1152/physrev.00019.2008, PMID: 19126760
30. Kawaguchi SY, Hirano T. (2007) **Sustained structural change of GABA(A) receptor-associated protein underlies long-term potentiation at inhibitory synapses on a cerebellar Purkinje neuron** *Journal of Neuroscience Research* **27**:6788-99. DOI: https://doi.org/10.1523/JNEUROSCI.1981-07.2007, PMID: 17581966
31. Kawaguchi SY, Sakaba T. (2015) **Control of inhibitory synaptic outputs by low excitability of axon terminals revealed by direct recording** *Neuron* **85**:1273–1288. DOI: https://doi.org/10.1016/j.neuron.2015.02.013, PMID: 25728570
32. Kew JN, Ducarre JM, Pflimlin MC, Mutel V, Kemp JA. (2001) **Activity-dependent presynaptic autoinhibition by group II metabotropic glutamate receptors at the perforant path inputs to the dentate gyrus and CA1** *Neuropharmacology* 40:20-27. DOI: https://doi.org/10.1016/s0028-3908(00)00118-0, PMID: 11077067
33. Khan AA, Shekh-Ahmad T, Khalil A, Walker MC, Ali AB. (2018) **Cannabidiol exerts antiepileptic effects by restoring hippocampal interneuron functions in a temporal lobe epilepsy model** *British Journal of Pharmacology* **175**:2097–2115. DOI: https://doi.org/10.1111/bph.14202, PMID: 29574880
34. Kim SH, Ryan TA. (2010) **CDK5 serves as a major control point in neurotransmitter release** *Neuron* **67**:797-809. DOI: https://doi.org/10.1016/j.neuron.2010.08.003, PMID: 20826311
35. Kreitzer AC, Regehr WG. (2001) **Retrograde inhibition of presynaptic calcium influx by**

endogenous cannabinoids at excitatory synapses onto Purkinje cells *Neuron* **29**:717–727. DOI: https://doi.org/10.1016/s0896-6273(01)00246-x, PMID: 11301030
36. Kushmerick C, Price GD, Taschenberger H, Puente N, Renden R, Wadiche JI, Duvoisin RM, Grandes P, von Gersdorff H. (2004) **Retroinhibition of Presynaptic Ca2+ Currents by Endocannabinoids Released via Postsynaptic mGluR Activation at a Calyx Synapse** *The Journal of Neuroscience* **24**:5955. DOI: https://doi.org/10.1523/JNEUROSCI.0768-04.2004, PMID: 15229243
37. Lee JS, Ho WK, Lee SH. (2012) **Actin-dependent rapid recruitment of reluctant synaptic vesicles into a fast-releasing vesicle pool** *PNAS* **109**:765-774. DOI: https://doi.org/10.1073/pnas.1114072109, PMID: 22393020
38. Mori Y, Takenaka KI, Fukazawa Y, Takamori S. (2021) **The endosomal Q-SNARE, Syntaxin 7, defines a rapidly replenishing synaptic vesicle recycling pool in hippocampal neurons** *Communications Biology* **4**:981. DOI: https://doi.org/10.1038/s42003-021-02512-4, PMID: 34408265
39. Midorikawa M, Sakamoto H, Nakamura Y, Hirose K, Miyata M. (2024) **Developmental refinement of the active zone nanotopography and axon wiring at the somatosensory thalamus** *Cell Reports* **43**:114770. DOI: https://doi.org/10.1016/j.celrep.2024.114770, PMID: 39321021
40. Miki T, Malagon G, Pulido C, Llano I, Neher E, Marty A. (2016) **Actin- and Myosin-Dependent Vesicle Loading of Presynaptic Docking Sites Prior to Exocytosis** *Neuron* **91**:808-823. DOI: https://doi.org/10.1016/j.neuron.2016.07.033, PMID: 27537485
41. Neher E, Marty A. (1982) **Discrete changes of cell membrane capacitance observed under conditions of enhanced secretion in bovine adrenal chromaffin cells** *PNAS* **79**:6712–6716. DOI: https://doi.org/10.1073/pnas.79.21.6712, PMID: 6959149
42. Nicholson-Tomishima K, Ryan TA. (2004) **Kinetic efficiency of endocytosis at mammalian CNS synapses requires synaptotagmin I** *PNAS* **101**:16648-16652. DOI: https://doi.org/10.1073/pnas.0406968101, PMID: 15492212
43. Ohno-Shosaku T, Maejima T, Kano M. (2001) **Endogenous cannabinoids mediate retrograde signals from depolarized postsynaptic neurons to presynaptic terminals** *Neuron* **29**:729–738. DOI: https://doi.org/10.1016/s0896-6273(01)00247-1, PMID: 11301031
44. Oka S, Nakajima K, Yamashita A, Kishimoto S, Sugiura T. (2007) **Identification of GPR55 as a lysophosphatidylinositol receptor** *Biochemical and Biophysical Research Communications* **362**:928-934. DOI: https://doi.org/10.1016/j.bbrc.2007.08.078, PMID: 17765871
45. Oka S, Toshida T, Maruyama K, Nakajima K, Yamashita A, Sugiura T. (2009) **2-Arachidonoyl-sn-glycero-3-phosphoinositol: a possible natural ligand for GPR55** *The Journal of Biochemistry* **145**:13-20. DOI: https://doi.org/10.1093/jb/mvn136, PMID: 18845565
46. Ramírez-Franco J, Bartolomé-Martín D, Alonso B, Torres M, Sánchez-Prieto J. (2014) **Cannabinoid type 1 receptors transiently silence glutamatergic nerve terminals of cultured cerebellar granule cells** *PLoS One* **9**:e88594. DOI: https://doi.org/10.1371/journal.pone.0088594, PMID: 24533119
47. Rosenberg EC, Chamberland S, Bazelot M, Nebet ER, Wang X, McKenzie S, Jain S, Greenhill S, Wilson M, Marley N, Salah A, Bailey S, Patra PH, Rose R, Chenouard N, Sun SD, Jones D, Buzsáki G, Devinsky O, Woodhall G, Scharfman HE, Whalley BJ, Tsien RW. (2023) **Cannabidiol modulates excitatory-inhibitory ratio to counter hippocampal hyperactivity** *Neuron* **111**:1282-1300.e8. DOI: https://doi.org/10.1016/j.neuron.2023.01.018, PMID: 36787750
48. Ryberg E, Larsson N, Sjögren S, Hjorth S, Hermansson NO, Leonova J, Elebring T, Nilsson K, Drmota T, Greasley PJ. (2007) **The orphan receptor GPR55 is a novel cannabinoid receptor** *British Journal of Pharmacology* **152**:1092-1101. DOI: https://doi.org/10.1038/sj.bjp.0707460, PMID: 17876302
49. Sankaranarayanan S, De Angelis D, Rothman JE, Ryan TA. (2000) **The use of pHluorins for optical measurements of presynaptic activity** *Biophysical Journal* **79**:2199-2208. DOI: https://doi.org/10.1016/S0006-3495(00)76468-X, PMID: 11023924
50. Sankaranarayanan S, Ryan TA. (2000) **Real-time measurements of vesicle-SNARE recycling in synapses of the central nervous system** *Nature Cell Biology* **2**:197-204. DOI: https://doi.org/10.1038/35008615, PMID: 10783237
51. Schneggenburger R, Neher E. (2000) **Intracellular calcium dependence of transmitter release rates at a fast central synapse** *Nature* **406**:889-893. DOI:

https://doi.org/10.1038/35022702, PMID: 10972290
52. Shallcross J, Hámor P, Bechard AR, Romano M, Knackstedt L, Schwendt M. (2019) **The Divergent Effects of CDPPB and Cannabidiol on Fear Extinction and Anxiety in a Predator Scent Stress Model of PTSD in Rats** *Frontiers in Behavioral Neuroscience* **13**:91. DOI: https://doi.org/10.3389/fnbeh.2019.00091, PMID: 31133832
53. Takahashi T, Kajikawa Y, Tsujimoto T. (1998) **G-Protein-coupled modulation of presynaptic calcium currents and transmitter release by a GABAB receptor** *The Journal of Neuroscience* **18**:3138-3146. DOI: https://doi.org/10.1523/JNEUROSCI.18-09-03138.1998, PMID: 9547222
54. Uusisaari M, Obata K, Knöpfel T. (2006) **Morphological and electrophysiological properties of GABAergic and non-GABAergic cells in the deep cerebellar nuclei** *Journal of Neurophysiology* **97**:901-911. DOI: https://doi.org/10.1152/jn.00974.2006, PMID: 17093116
55. Vyleta NP, Jonas P. (2014) **Loose coupling between Ca^{2+} channels and release sensors at a plastic hippocampal synapse** *Science* **343**:665-670. DOI: https://doi.org/10.1126/science.1244811, PMID: 24503854
56. Weisskopf MG, Castillo PE, Zalutsky RA, Nicoll RA. (1994) **Mediation of hippocampal mossy fiber long-term potentiation by cyclic AMP** *Science* **265**:1878–1882. DOI: https://doi.org/10.1126/science.7916482, PMID: 7916482
57. Wilson RI, Nicoll RA. (2001) **Endogenous cannabinoids mediate retrograde signalling at hippocampal synapses** *Nature* **410**:588–592. DOI: https://doi.org/10.1038/35069076, PMID: 11279497
58. Wu CS, Chen H, Sun H, Zhu J, Jew CP, Wager-Miller J, Straiker A, Spencer C, Bradshaw H, Mackie K, Lu HC. (2013) **GPR55, a G-protein coupled receptor for lysophosphatidylinositol, plays a role in motor coordination** *PLoS One* **8**:e60314. DOI: https://doi.org/10.1371/journal.pone.0060314, PMID: 23565223
59. Wu Y, Liu Q, Guo B, Ye F, Ge J, Xue L. (2020) **BDNF Activates Postsynaptic TrkB Receptors to Induce Endocannabinoid Release and Inhibit Presynaptic Calcium Influx at a Calyx-Type Synapse** *The Journal of Neuroscience* **40**:8070-8087. DOI: https://doi.org/10.1523/JNEUROSCI.2838-19.2020, PMID: 3294867
60. Yamashita M, Kawaguchi SY, Hori T, Takahashi T. (2018) **Vesicular GABA Uptake Can Be Rate Limiting for Recovery of IPSCs from Synaptic Depression** *Cell Rep*orts. **22**:3134-3141. DOI: https://doi.org/10.1016/j.celrep.2018.02.080, PMID: 29562170
61. Zorrilla de San Martin J, Trigo FF, Kawaguchi SY. (2017) **Axonal GABAA receptors depolarize presynaptic terminals and facilitate transmitter release in cerebellar Purkinje cells** *The Journal of Physiology* **595**:7477-7493. DOI: https://doi.org/10.1113/JP275369, PMID: 29072780

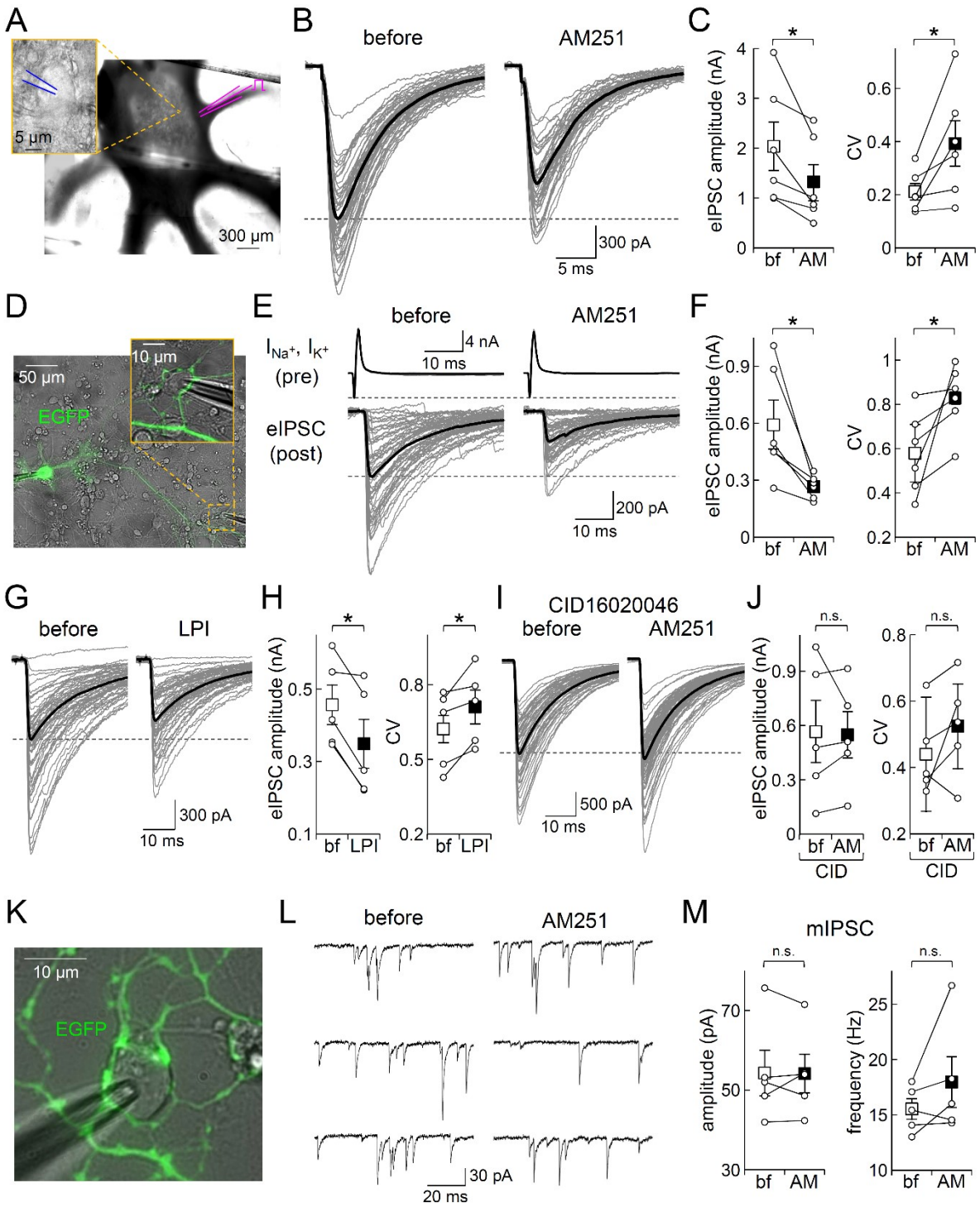

Figure 1. Reduced transmission at PC-DCN synapses by GPR55

(**A**) Image of patch-clamp recordings from a DCN neuron in slice. A magnified image of the recorded neuron is shown as inset (patch pipette is indicated in blue). A pipette for electrical stimulation (magenta) was placed at the white matter. (**B, C**) Individual (gray) and averaged (black) traces (B), amplitudes (C, left, open and filled squares) and CV (C, right) of eIPSCs before and after application of AM251 in slices (n = 6). Open circles connected by lines represent individual cells. (**D**) Image of dual whole-cell recordings from a presynaptic EGFP-labeled PC soma and its postsynaptic target neuron in cerebellar culture. (**E-J**) Representative traces (E, G, I), amplitude and CV (F, H, J) of eIPSCs at a postsynaptic cell before and after application of AM251 (E, F, n = 6), LPI (G, H, n = 5), or AM251 in the presence of CID (I, J, n = 5). In E, presynaptic Na^+ and the following K^+ currents (I_{Na^+}, I_{K^+}) at a presynaptic PC soma are also shown. (**K**) Image of mIPSC recordings from a neuron innervated by lots of EGFP-positive PC boutons in culture. (**L, M**) Representative traces (L), amplitude and frequency (M) of mIPSCs before and after the AM251 application. n = 5 cells. Data are mean ± SEM. * $p < 0.05$; n.s., not significant.

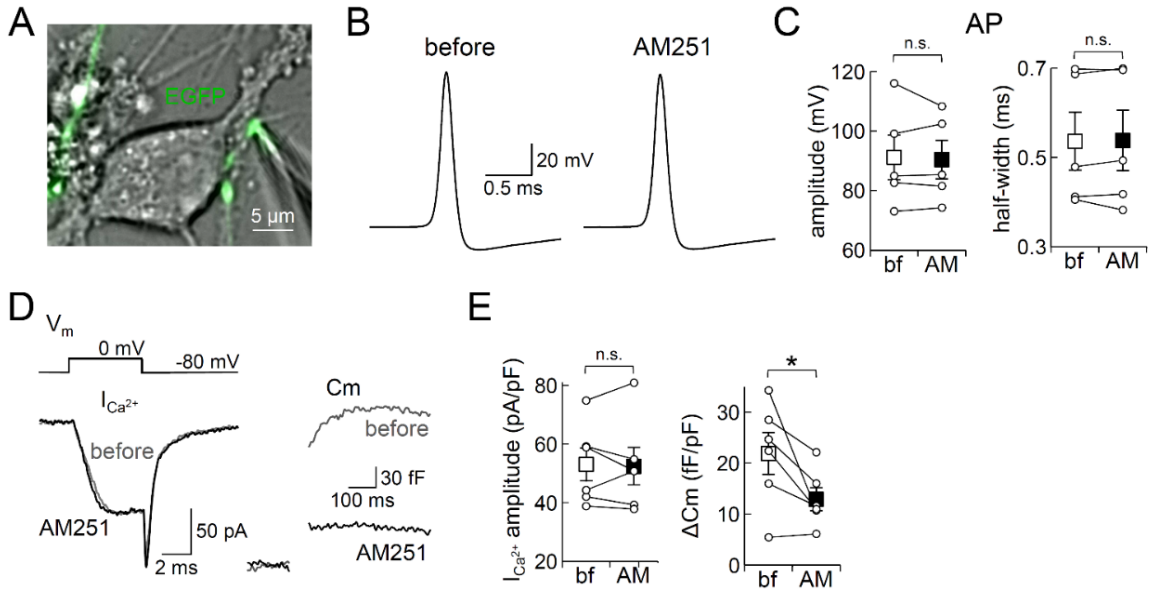

Figure 2. Reduced vesicle exocytosis by GPR55 without changing presynaptic Ca^{2+} influx
(**A**) Image of direct patch-clamp recording from an EGFP-labeled PC axon terminal in culture. (**B, C**) Representative traces (B), amplitude and half-height width (C) of APs recorded from PC terminals before and after the AM251 application. n = 5 boutons. (**D, E**) Representative traces (D) and amplitude (E) of presynaptic Ca^{2+} currents ($I_{Ca^{2+}}$) and Cm increase upon 5 ms depolarization before and after the AM251 application. n = 6 boutons. Both $I_{Ca^{2+}}$ and Cm increase were normalized by the size of presynaptic Cm under the voltage-clamp. Data are mean ± SEM. * $p < 0.05$; n.s., not significant.

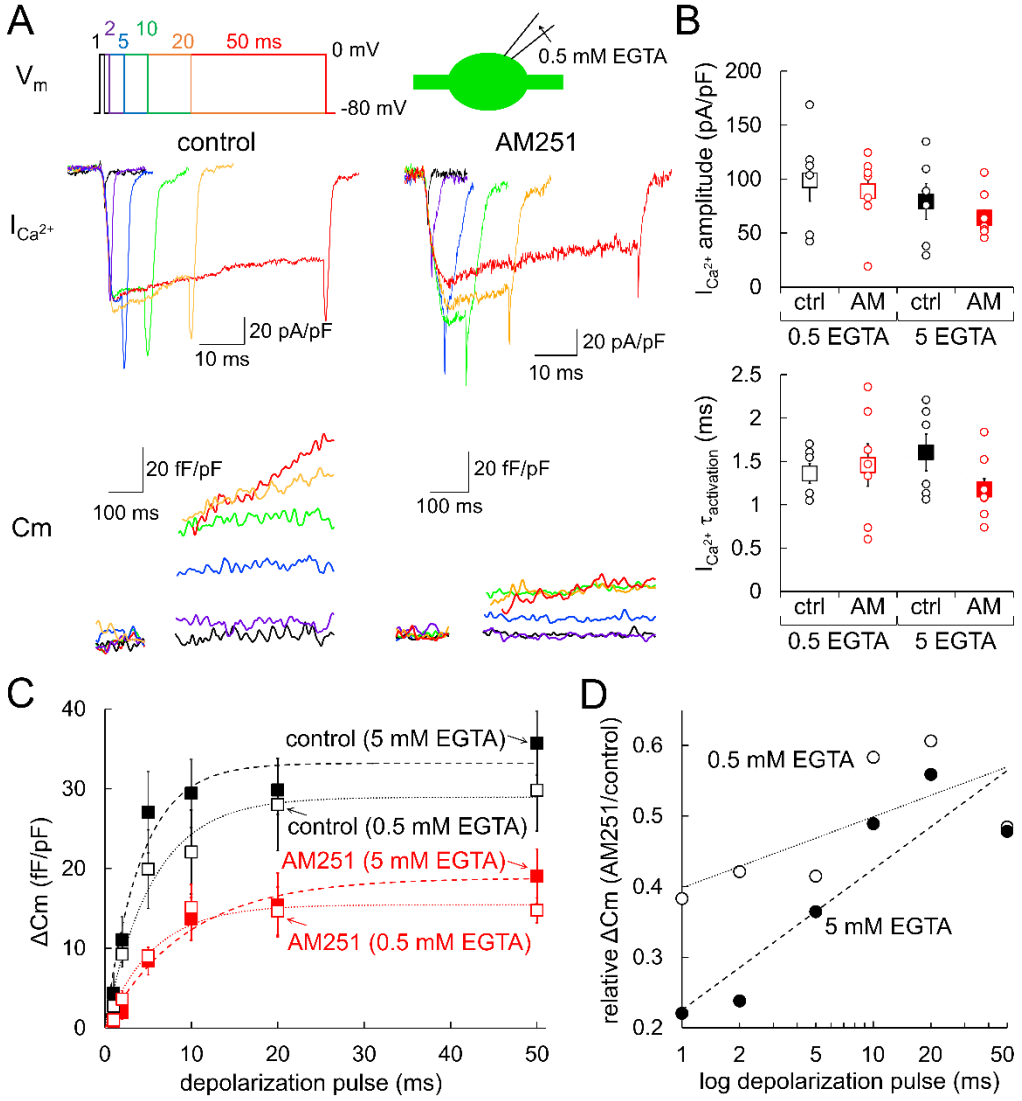

Figure 3. Decrease in RRP vesicles by GPR55

(**A**) Representative traces of presynaptic $I_{Ca^{2+}}$ (middle) and the resultant Cm increase (bottom) upon 1, 2, 5, 10, 20, or 50 ms of depolarization pulses (to 0 mV) (top) without (left) or with (right) AM251. Recordings were performed by a presynaptic patch pipette containing 0.5 mM EGTA. (**B**, **C**) Amplitude and time constant for activation of $I_{Ca^{2+}}$ (B), and Cm change (C) upon depolarization pulses recorded without (black, 0.5 mM EGTA, n = 6; 5 mM EGTA, n = 6) or with AM251 (red, 0.5 mM EGTA, n = 7; 5 mM EGTA, n = 8). Single exponential fits for each are shown as dotted lines. Both $I_{Ca^{2+}}$ and Cm change were normalized by the size of presynaptic Cm under the voltage-clamp. In B, data for individual cells (open circles) and mean ± SEM (squares) are shown. (**D**) Ratio of Cm increase (Cm increase with AM251 divided by that in control) recorded with 0.5 or 5 mM presynaptic EGTA is plotted against the duration of log depolarization pulse.

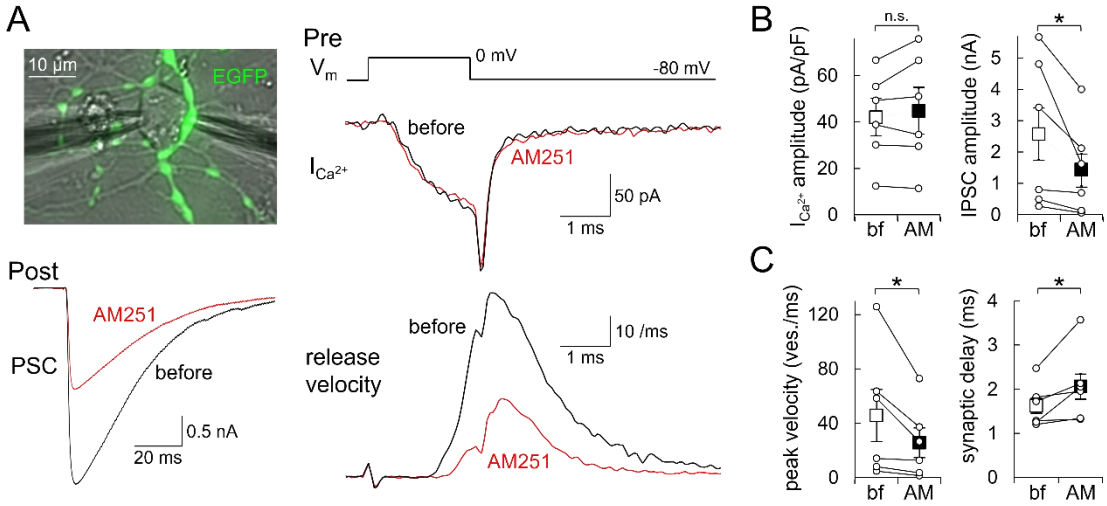

Figure 4. Halved velocity of exocytosis shown by pre- and postsynaptic paired recordings
(**A**) Image of paired recordings from a presynaptic EGFP-labeled PC bouton and its postsynaptic neuron (upper left), and representative traces of the presynaptic $I_{Ca^{2+}}$ (right middle), IPSC (lower left), and velocity of vesicular fusion (calculated by the deconvolution of IPSC trace) upon 2 ms depolarization before and after the AM251 application (right bottom). (**B, C**) Amplitude of I_{Ca2+} (B, left, calibrated by the presynaptic Cm under the voltage-clamp), IPSC (B, right), maximal release velocity (C, left) and synaptic delay (C, right) before and after (connected by lines) application of AM251. Data are mean ± SEM. * $p < 0.05$; n.s., not significant. n = 6 pairs.

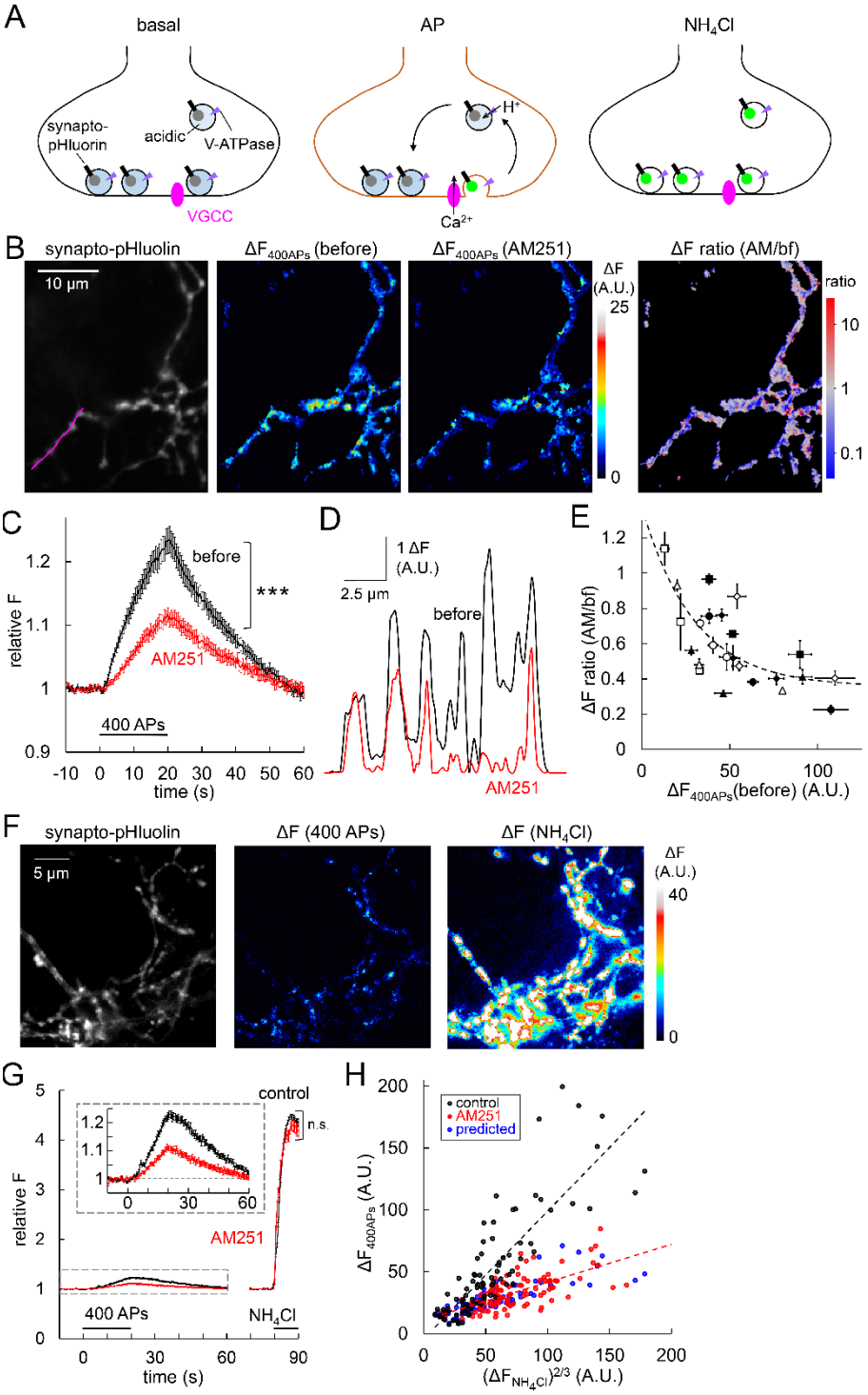

Figure 5. Halved vesicular releases by GPR55 imaged with pHluorin

(**A**) Schematic illustration of imaging of vesicle exocytosis with synapto-pHluorin. Upon vesicular fusion at the AP arrival, pHluorin becomes fluorescent because of exposure to the neutral pH. NH_4^+ application forcefully neutralizes vesicle lumen. (**B**) Representative images of synapto-pHluorin fluorescence and the color-coded fluorescence increase upon 400 APs (ΔF_{400APs}) in PC terminals before and after the AM251 application. The right-most panel shows the ratio of fluorescence increase after the AM251 application relative to that before, represented in pseudo-color. (**C**) Time courses of 400 APs-triggered pHluorin fluorescence changes before and after AM251 application. (**D**) Plot of ΔF_{400APs} along a PC axon (indicated as the magenta line in B) before and after the AM251 application. (**E**) Ratio of ΔF_{400APs} after the AM251 application relative to that before is plotted against the ΔF_{400APs} before the AM251 application. Data from different cells are shown as different symbols. n = 8 cells.

Dashed line represents data fitting with a function: $y = 1.02e^{-0.0334x} + 0.355$, $R^2 = 0.506$. (**F**) Images of pHluorin fluorescence and the color-coded fluorescence increases upon 400 APs and the following NH_4Cl application (50 mM) in a PC axon. (**G**) Time courses of synapto-pHluorin fluorescence changes upon 400 APs and the following NH_4Cl application without or with AM251. Inset shows enlarged traces. (**H**) ΔF_{400APs} is plotted against the ΔF caused by NH_4Cl (ΔF_{NH4Cl}) for individual boutons without or with AM251. The effect of AM251 was predicted (blue) by conversion of dataset for control (black) based on the relationship shown in E, showing similar distribution to the actual data obtained with AM251 (red). Fitted line for control: $y = 1.03x – 4.05$, $R^2 = 0.704$; for AM251, $y = 0.307 + 10.9$, $R^2 = 0.441$. Data are mean ± SEM. *** $p < 0.001$; n.s., not significant.

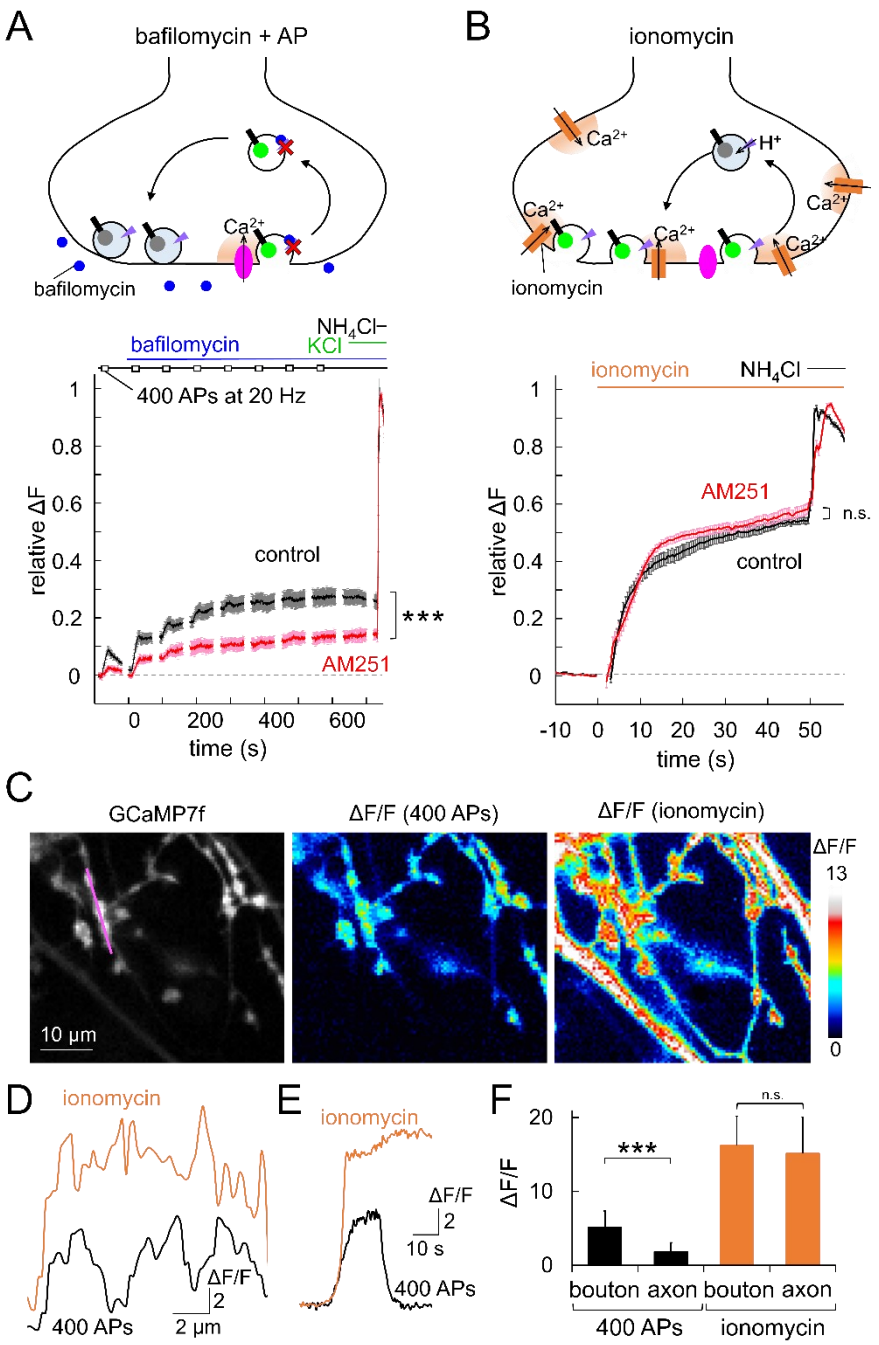

Figure 6. Increase of reluctant vesicle insensitive to APs by GPR55
(**A, B**) Schematic illustration (top) and time courses of synapto-pHluorin fluorescence changes upon the repetitive 400 APs trains (20 Hz) before and after application of bafilomycin and KCl (finally 50 mM) (A) or ionomycin (B), followed by the NH_4Cl application, in the presence or absence of AM251. Data are mean ± SEM. *** $p < 0.001$; n.s., not significant. (**C**) Fluorescent images of GCaMP7f expressed in PC axon terminals (left) and color-coded relative fluorescence increase (ΔF/F) upon 400 APs at 20 Hz (middle) or the following ionomycin application (right). (**D, E**) Distribution pattern in an axonal segment (D, along a magenta line indicated in C) and representative time course (E) at the middle bouton of ΔF/F caused by 400 APs or ionomycin. (**F**) ΔF/F of GCaMP7f at PC boutons (n = 20 boutons from 4 PCs) or axonal segments (n = 26 segments) upon 400 APs or application of ionomycin.

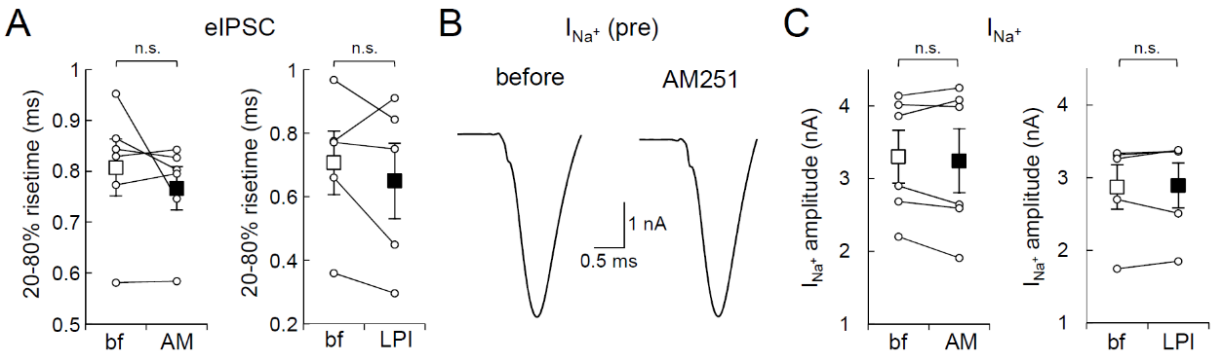

Figure S1. No effects of GPR55 on time courses of IPSCs and somatic Na^+ currents

(**A**) 20-80 % risetime of eIPSCs before and after application of AM251 (left, n = 6) or LPI (right, n = 5). Data for individual cells are also shown (open circles). (**B, C**) Representative traces (B) and amplitudes (C) of Na^+ current before and after application of AM251 or LPI. AM251, n = 6; LPI, n = 5. Data are mean ± SEM. n.s., not significant.

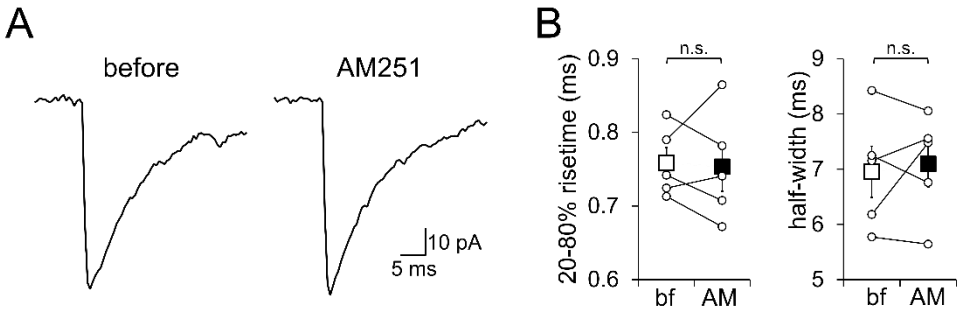

Figure S2. No effects of GPR55 on mIPSCs time courses

Representative averaged traces (from 20 events for each, A) and 20-80 % risetime or half-width (B) of mIPSCs before and after application of AM251 (n = 5). Data for individual cells are also shown (open circles). Data are mean ± SEM. n.s., not significant.

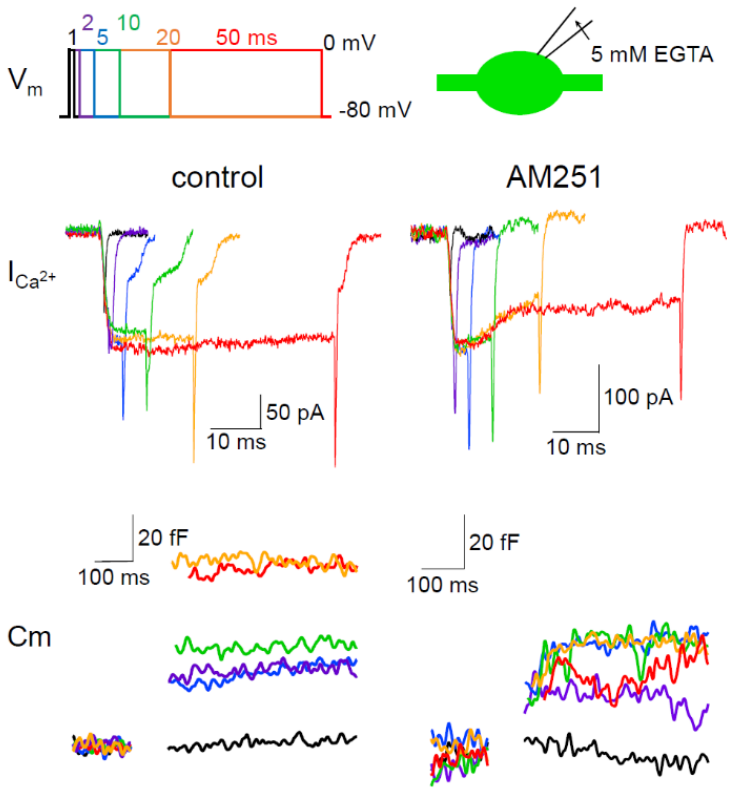

Figure S3. GPR55-mediated suppression of release in PC boutons with 5 mM EGTA
Representative traces of presynaptic $I_{Ca^{2+}}$ (middle) upon 1, 2, 5, 10, 20 and 50 ms of depolarization (to 0 mV, depicted on the top) of a PC bouton, and the resultant Cm increase (bottom) in the presence or absence of AM251. Recording was performed with a patch pipette containing 5 mM EGTA.

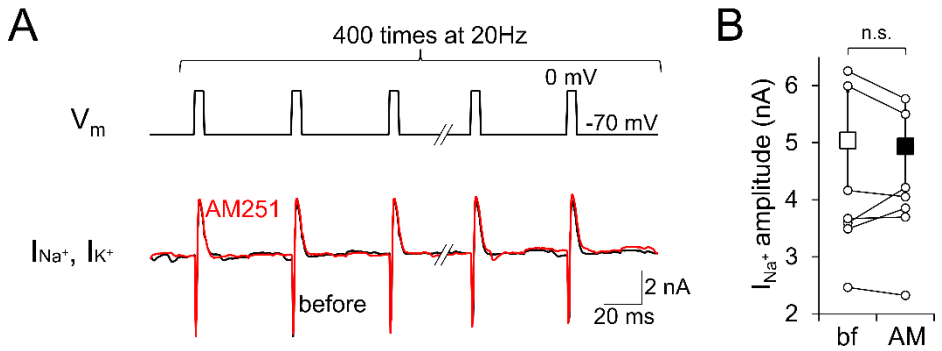

Figure S4. Repetitive somatic Na^+ currents unaffected by GPR55 activation

Representative traces (**A**) and amplitudes (**B**) of somatic Na^+ currents at 20Hz before and after application of AM251 (n = 7). In B, data for individual cells are also shown (open circles). Averaged data represent mean ± SEM. n.s., not significant.